Supplementary material:

Tensegrity-Based Legged Robot Generates Passive Walking, Skipping, and Crawling Gaits in Accordance with Environment

Yanqiu Zheng, Fumihiko Asano, Cong Yan, Longchuan Li,
and Isao T. Tokuda

This supplementary material discusses the following three issues.

- Eigen-frequency analysis of the rimless wheel-like tensegrity (RTW) model and normalization of the model parameters.
- Exploration of parameter space.
- Comparison of the RTW model to conventional locomotion models with a summary table extended from Table 1 of the main article.

1 Eigen-frequency analysis and parameter normalization

To systematically analyze the rimless wheel-like tensegrity (RTW) model, which can generate various movement patterns such as walking, crawling, and skipping, it is important to normalize the parameters. Such normalization may provide a criterion for designing the model parameters. First, we performed eigen-frequency analysis of the RTW model. Due to nonlinear nature of the collision dynamics as well as the internal coupling of the RTW model, an analytical solution cannot be directly derived. We therefore introduce an approximate model of the RTW and performed its linearization. Based on the linearized model, we derived its linear state space equations and obtained analytical solution for eigen-frequency and critical damping of the RTW model. Based on the eigen-frequency analysis, a scheme for normalizing the model parameters is introduced.

1.1 Approximate model of RTW

Although the RTW model has 9 degrees of freedom, experimental observations suggest that the RTW movement is primarily driven by rotation of the three

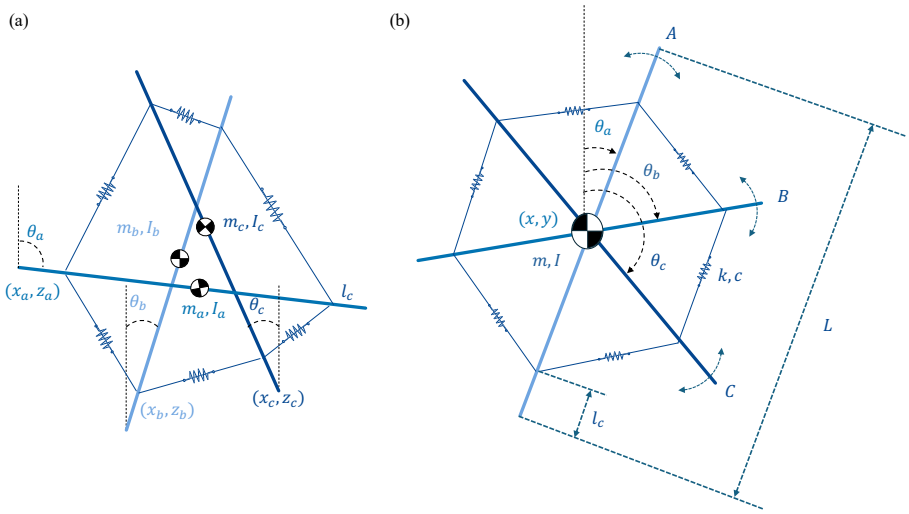

Figure S1: (a) Proposed RTW model, (b) Approximate model of RTW, consisting of three rods with length L, mass m, and moment of inertia I, whose center is constrained at (x, y) and can rotate freely. These rods are connected by six massless elastic strings, where the distance from the connection point to the tip of each rod is l_c.

rods, with the motion mainly occurring around the central point. To simplify the model and approximate its motion, we introduce an approximate model of the RTW as shown in Fig. S1. Compared to the original RTW model, it only considers the rotation of each rod, ignoring the translational motion on the plane. This approximate model reduces the degrees of freedom only to three, which correspond to the angles of the three rods.

1.2 Equation of motion

To calculate eigen-frequency of the approximate model, we neglect the effect of gravity and let $\boldsymbol{q} = \begin{bmatrix} \theta_a & \theta_b & \theta_c \end{bmatrix}^{\mathrm{T}}$ be the generalized coordinates. Then the equation of motion for the approximate model is given by:

$$\boldsymbol{M}\ddot{\boldsymbol{q}} = \boldsymbol{F}, \tag{S1}$$

where the inertia matrix $\boldsymbol{M}$ and the moment of inertia I are

$$\boldsymbol{M} = \begin{bmatrix} I & 0 & 0 \\ 0 & I & 0 \\ 0 & 0 & I \end{bmatrix}, \tag{S2}$$

$$I = mL^2/12. \tag{S3}$$

On the right-hand side of Eq. (S1), $\boldsymbol{F}$ represents coupling tensions (detailed in Section 2C of the main article), which can be decomposed into:

$$\boldsymbol{F} = \boldsymbol{F}_k + \boldsymbol{F}_c, \tag{S4}$$

where

$$\boldsymbol{F}_k = \begin{bmatrix} 2k((L-2l_c)/2)^2(\sin(\theta_a-\theta_b)-\sin(\theta_a-\theta_c)) \\ 2k((L-2l_c)/2)^2(-\sin(\theta_a-\theta_b)+\sin(\theta_b-\theta_c)) \\ 2k((L-2l_c)/2)^2(\sin(\theta_a-\theta_c)-\sin(\theta_b-\theta_c)) \end{bmatrix}, \tag{S5}$$

$$\boldsymbol{F}_c = \begin{bmatrix} -c((L-2l_c)/2)^2(-2\dot{\theta}_a+\dot{\theta}_b+\dot{\theta}_c+(-\dot{\theta}_a+\dot{\theta}_b)\cos(\theta_a-\theta_b)+(\dot{\theta}_a-\dot{\theta}_c)\cos(\theta_a-\theta_c)) \\ -c((L-2l_c)/2)^2(\dot{\theta}_a-2\dot{\theta}_b+\dot{\theta}_c+(\dot{\theta}_a-\dot{\theta}_b)\cos(\theta_a-\theta_b)+(-\dot{\theta}_b+\dot{\theta}_c)\cos(\theta_b-\theta_c)) \\ c((L-2l_c)/2)^2(-\dot{\theta}_a-\dot{\theta}_b+2\dot{\theta}_c+(\dot{\theta}_a-\dot{\theta}_c)\cos(\theta_a-\theta_c)+(-\dot{\theta}_b+\dot{\theta}_c)\cos(\theta_b-\theta_c)) \end{bmatrix}. \tag{S6}$$

1.3 Linearization

To obtain an analytical solution, we linearize the approximate model. Specifically, sine and cosine terms in Eqs. (S5) and (S6) are linearlized. Taking $\sin(\theta_a-\theta_b)$ as an example, the sine terms are linearlized as:

$$\begin{aligned} &\sin(\theta_a-\theta_b) \\ =&\sin(-3/\pi+(\theta_a-\theta_b+3/\pi)) \\ =&\sin(-3/\pi)\cos(\theta_a-\theta_b+3/\pi)+\cos(-3/\pi)\sin(\theta_a-\theta_b+3/\pi). \end{aligned} \tag{S7}$$

Assuming the shape shown in Fig. S1(b) as the equilibrium position, which holds the relation of $\theta_a^*-\theta_b^*=-3/\pi$, then

$$(\theta_a-\theta_b+3/\pi)\Big|_{\theta_a=\theta_a^*,\theta_b=\theta_b^*}=0. \tag{S8}$$

Substituting Eq. (S8) into Eq. (S7) and applying the Taylor expansion, we obtain:

$$\sin(\theta_a-\theta_b)\approx\sin(-3/\pi)+\cos(-3/\pi)(\theta_a-\theta_b+3/\pi). \tag{S9}$$

In a similar manner, the cosine terms are linearlized as:

$$\begin{aligned} &\cos(\theta_a-\theta_b) \\ =&\cos(-3/\pi+(\theta_a-\theta_b+3/\pi)) \\ =&\cos(-3/\pi)\cos(\theta_a-\theta_b+3/\pi)-\sin(-3/\pi)\sin(\theta_a-\theta_b+3/\pi) \\ \approx&\cos(-3/\pi)-\sin(-3/\pi)(\theta_a-\theta_b+3/\pi) \\ \approx&\cos(-3/\pi). \end{aligned} \tag{S10}$$

Substituting Eqs. (S9) and (S10) into Eq. (S4), we obtain the linearized equations of motion as

$$\boldsymbol{M}\ddot{\boldsymbol{q}} = \boldsymbol{F}_l, \tag{S11}$$

where $\boldsymbol{F}_l$ represents the linearized $\boldsymbol{F}$.

1.4 Eigen-frequencies

The second-order equation of motion (S11) can be transformed to the first-order state-space equation as

$$\dot{\boldsymbol{X}} = \boldsymbol{A}\boldsymbol{X}, \tag{S12}$$

where $\boldsymbol{X} = \begin{bmatrix} \boldsymbol{q}^{\mathrm{T}} & \dot{\boldsymbol{q}}^{\mathrm{T}} \end{bmatrix}^{\mathrm{T}}$ and

$$\boldsymbol{A} = \begin{bmatrix} 0 & 0 & 0 & 1 & 0 & 0 \\ 0 & 0 & 0 & 0 & 1 & 0 \\ 0 & 0 & 0 & 0 & 0 & 1 \\ (\boldsymbol{M}^{-1}\boldsymbol{F}_l)/\partial \boldsymbol{X}^{\mathrm{T}} \end{bmatrix}. \tag{S13}$$

Eigenvalues $\boldsymbol{\lambda}$ of the motion matrix $\boldsymbol{A}$ can be derived as follows:

$$\boldsymbol{\lambda} = \begin{bmatrix} 0 \\ 0 \\ \dfrac{(5c((L-2l_c)/2)^2 - \sqrt{-16Ik((L-2l_c)/2)^2 + 25c^2((L-2l_c)/2)^4}}{4I} \\ \dfrac{(5c((L-2l_c)/2)^2 + \sqrt{-16Ik((L-2l_c)/2)^2 + 25c^2((L-2l_c)/2)^4}}{4I} \\ \dfrac{(9c((L-2l_c)/2)^2 - \sqrt{3}\sqrt{16Ik((L-2l_c)/2)^2 + 27c^2((L-2l_c)/2)^4}}{4I} \\ \dfrac{(9c((L-2l_c)/2)^2 + \sqrt{3}\sqrt{16Ik((L-2l_c)/2)^2 + 27c^2((L-2l_c)/2)^4}}{4I} \end{bmatrix}. \tag{S14}$$

If the eigenvalues include complex roots, they indicate oscillatory solutions. We observe that the eigenvalues for the 1st, 2nd, 5th, and 6th components are real numbers. However, if the quantity underneath the square root sign for the 3rd and 4th components is negative, complex roots appear. Thus ciritical condition for the oscillatory solution is:

$$-16Ik((L-2l_c)/2)^2 + 25c^2((L-2l_c)/2)^4 < 0. \tag{S15}$$

After simplification and reorganization, the expression becomes:

$$c < c_c, \tag{S16}$$

where the critical damping coefficient is given by

$$c_c = \frac{4}{5}\sqrt{\frac{Ik}{(L-2l_c)^2/4}}. \tag{S17}$$

Without damping (*i.e.*, $c = 0$), the eigen-frequency f_n is:

$$f_n = \frac{(L-2l_c)}{4\pi}\sqrt{\frac{k}{I}}. \tag{S18}$$

1.5 Parameter Normalization

Based on the eigen-frequency analysis, the model parameters are normalized. The RTW model includes the following structural parameters: rod mass m, connection position l_c, elastic coefficient k, and damping coefficient c. By using the rod length L as the basis parameter, the four parameters (m, l_c, k, c) are normalized as follows.

1. Assuming that the rod mass is proportional to its length (assuming that the cross-sectional area is constant), the mass can be expressed as

$$m = \rho L, \tag{S19}$$

   where ρ represents the density.

2. The connection position l_c can be described as

$$l_c = \alpha L \tag{S20}$$

   using α as its ratio to the rod length L.

3. Based the eigen-frequency f_n of Eq. (S18), the stiffness k can be represented as

$$k = f_n^2 \frac{(4\pi)^2 I}{(L-2l_c)^2} = \frac{4\pi^2}{3} \frac{\rho f_n^2}{(1-2\alpha)^2} L. \tag{S21}$$

4. Finally, using the critical damping coefficient c_c of Eq. (S17), the damping coefficient can be described as

$$c = \zeta c_c = \zeta \frac{4}{5} \sqrt{\frac{Ik}{(L-2l_c)^2/4}} = \frac{8\pi}{15} \frac{\zeta \rho f_n}{(1-2\alpha)^2} L, \tag{S22}$$

   where ζ represents the damping ratio.

1.6 Simulation Results

To examine the validity of the eigen-frequency analysis, the RTW model was simulated based on the normalized parameters. First, the normalized parameter values were set to $L = 0.8$, $\rho = 2.5$, $\alpha = 0.125$, $\zeta = 0.0514$, $\phi = 0.15$, which correspond to the walking gait shown in Fig. 7(a) of the main article. By changing the eigen-frequency from $f_n = 2$ Hz to 5 Hz, the RTW model was simulated and the averaged walking frequency f_w of successfully simulated gaits was plotted in Fig. S2. The walking frequency of the simulated RTW is very close to the eigen-frequency (*i.e.*, $f_n \approx f_n$), indicating that the eigen-frequency derived from the approximate model captures dynamical characteristics of the RTW model quite well.

Next, to examine the efficiency of the parameter normaliation, we have reproduced Fig. 7 (a) of the main article. We fixed the normalized parameter values to $\rho = 2.5$, $\alpha = 0.125$, $f_n = 3.269$, $\zeta = 0.0514$ and simulated the walking

gait by varying the slope from $\phi = 0.05$ to 0.2 rad in Fig. S3. Proportions of single-leg support phase (blue) and double-leg support phase (red) remain close to 50 % for the variable slope. Moreover, similar curves are drawn for different values of the rod length $L = 0.7, 0.8, 0.9$, indicating that the gait characteristics are preserved across different rod lengths.

2 Exploration of Parameter Space

To examine whether the gait patterns studied in the main article are not due to specific selection of the parameter values, we explored other parameter settings of the RTW model. We fixed the rod length to $L = 0.8$, randomized the normalized parameter values in the range of $\rho \in [1, 5]$, $\alpha \in [0, 0.4]$, $f_n \in [1.5, 5]$, $\zeta \in [0.05, 0.1]$, $\phi \in [0.05, 0.3]$, and checked whether stable gaits are achieved. Among 1000 sets of randomly selected parameter values, stable gaits were observed for 73.7 %, within which skipping, walking, and crawling gaits were observed for 35.9 %, 32 %, 5.8 %, respectively. This indicates that the three types of passive gaits are observed in a wide range of the parameter space. The RTW dynamics studied in the main article is not specific to restricted parameter values.

Next, we explored the parameter setting, in which no stable gaits were observed (blue dots in Fig. S4). According to our inspection, the gait failure

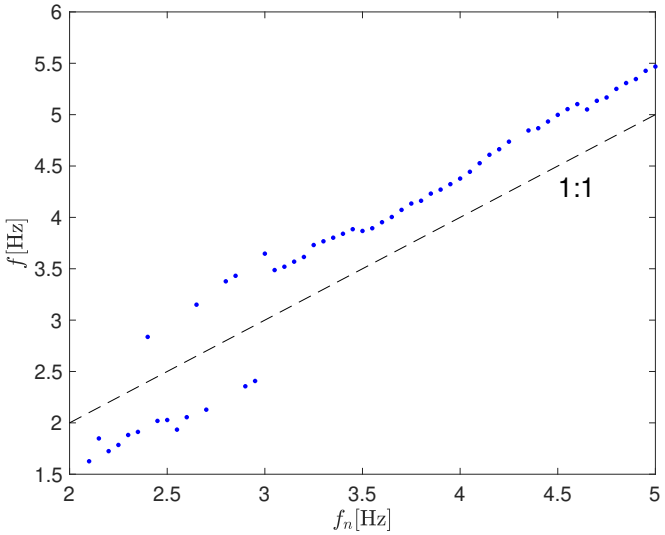

Figure S2: Dependence of the walking frequency f_w of the simulated RTW model on the eigen-frequency f_n. The points located close to the diagonal line implies that the walking frequency is well approximated by the eigen-frequency f_n.

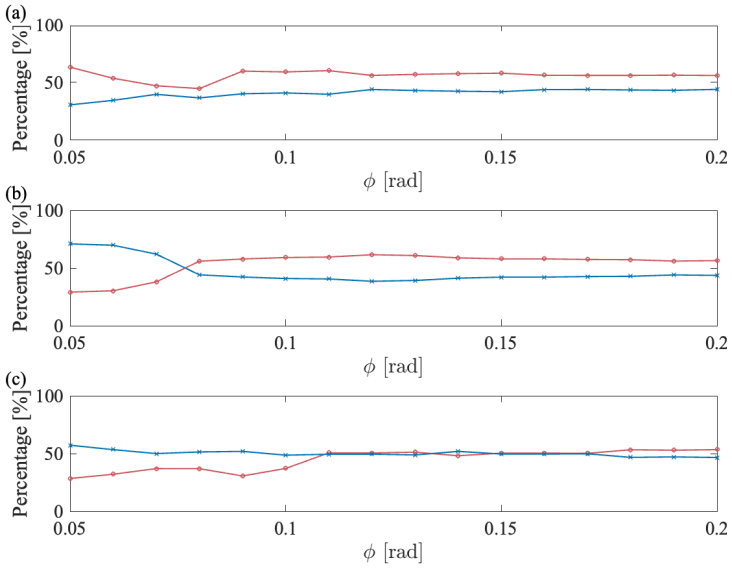

Figure S3: Gait transitions induced by the increasing slope ϕ. In each diagram, time-intervals, during which the ground contact states appear, are drawn in percentage (blue: single-leg support phase, red: double-leg support phase). The rod length was set to (a) $L = 0.7$ m, (b) $L = 0.8$ m (same as Fig. 7(a) in the main paper), and (c) $L = 0.9$m, while the normalized parameters were set commonly to $(\alpha, f_n, \zeta) = (0.125, 3.269, 0.0514)$. For different rod lengths, consistent gait patterns are observed.

seemed rather independent of the the mass coefficient ρ and the damping ratio ζ in the randomized ranges. In contrast, ratio of connection position to rod length α, eigen-frequency f_n, and slope ϕ showed a clear influence on the gait failure. Figure S4) shows that the failed gaits form two distinct clusters. The first cluster (shown on the left side of Fig. S4(a)) indicates the cases, in which the gait failed due to insufficient stiffness (small α and low f_n), that cannot maintain standing position of the RTW model, leading to its structural collapse. The second cluster (shown on the right side of Fig. S4(a)) represents the cases, in which the RTW model cannot overcome the potential energy barrier because of insufficient gravitational energy (small ϕ). As the slope ϕ increases, this region disappears because more gravitational energy is supplied. When deigning the RTW, these two parameter regions should be avoided.

In summary, the parameter space exploration demonstrated that the RTW failed to achieve stable gait primarily in two scenarios: (1) structural collapse due to insufficient stiffness and (2) incapability of overcoming the energy barriers under low gravitational energy. These findings suggest that the gait failures can be avoided by adjusting the stiffness (*i.e.*, f_n) and gravitational energy (*i.e.*, ϕ). This provides practical guidelines for designing the RTW model for practical

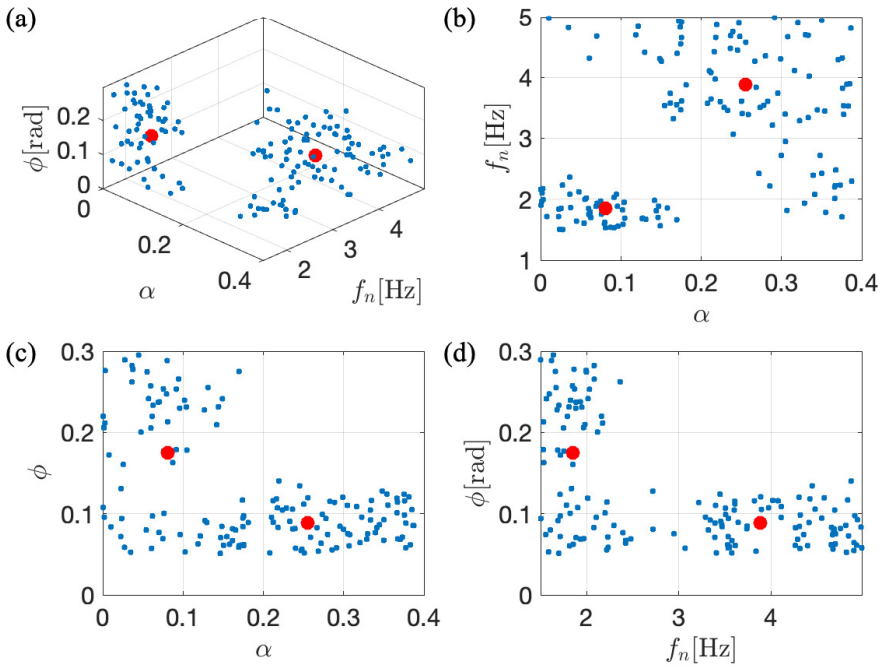

Figure S4: Parameter settings, in which the RTW model failed to generate stable gaits, are drawn as blue points in (a) 3-dimensional space (α, f_n, ϕ), (b) 2-dimensional space (α, f_n), (c) 2-dimensional space (α, ϕ), (d) 2-dimensional space (f_n, ϕ). The distributed points form two distinct clusters, with red point marking the center of each cluster.

applications.

3 Comparison to conventional models

To highlight the key features of the RTW model, Table S1 compares the RTW with four types of conventional locomotion models: inverted pendulum (IP), spring-loaded inverted pendulum (SLIP), RW, and biomechanical models. Simplicity of the model was measured as the number of degrees of freedom (DOF) and the number of model parameters, while generality of the model was evaluated as the number of different types of generated gaits.

The biomechanical models tend to have a large number of DOF and parameters to capture complex movements of animals [1, 2, 3]. For instance, to reproduce detailed movements of a horse, the model takes into account interaction between many parts of the horse's body. While a large number of DOF and more parameters lead to a more accurate description of the motion, such systems are known to have a limited capability of generalization [4, 5]. This implies

that, once the parameters are tuned to a specific gait, the model may generate only the corresponding gait, where extensive changes in model structure and parameters are needed to produce different gait patterns.

The IP has only one DOF, reflecting the motion of the center of mass (CoM) in the single-legged-support-phase (SLSP) of bipedal locomotion [6]. In quadrupedal locomotion, the IP can represent motion of either front or rear leg during SLSP. It is, however, difficult to generate natural continuous gaits due to its lack of collision dynamics.

The RW not only possesses dynamical characteristics of the IP under SLSP but it also introduces collisions, which determine the next initial state and thus enable generation of natural continuous gait [7]. This requires two additional DOFs to describe the positioning. Due to the rigid characteristics, neither IP nor RW can represent motion states like double-legged-support-phase (DLSP). Because of such restriction, IP and RW can produce only walking gait.

Concerning the SLIP models, which introduced elasticity to the rigid IP model, they have a small number of DOF and parameters, enabling their simulations with a low computational cost. By designing the model structure with multiple legs, various movements, such as bipedal, quadrupedal, and hexapod gaits, can be realized [8, 9, 10, 11, 12, 13, 14, 15, 16, 17, 18, 19]. However, as shown in Table S1, each gait is composed of multiple motion states, where a single set of parameters can represent only one motion state. Consequently, additional sets of parameters are required to describe more complex gait patterns. For instance, biped walking is composed of two motion states: SLSP and DLSP. To generate an idealistic gait (*e.g.*, symmetric gaits and symmetric legs), only a single set of parameters is enough (6 parameters shown in Table S1). In the case of asymmetric gaits or asymmetric legs, however, two motion states with different sets of parameters are required, thus 5 (for SLSP) + 6 (for DLSP) parameters are needed. Another note is that the conditions for switching the motion states, such as the touchdown angle, need to be manually set [8]. The touchdown angle not only determines the landing state but it also affects the initial state of the next step. Manually setting such parameters may produce physically unrealistic movement and may not precisely account for the energy loss during the collision [9]. For this reason, system properties such as bifurcations, which may naturally occur in nonlinear systems [20], would not be easily produced.

The RTW model has a relatively high DOF because each rod has 3 DOF. In the equations of motion, the collision effect is considered, where a physically realistic switching of the stance and swing legs is realized, and the associated energy loss is also considered. The RTW has 6 parameters including the external environmental parameter ϕ and the internal coupling strength k. Unlike the SLIP model, the motion states are not determined by the parameters but are described by the equations of motion. Thus, relatively few parameters are needed to simulate complex gaits. Because of the physically realistic dynamics and the few parameters (*i.e.*, higher generalization capability), the RTW is capable of generating various gaits with a slight change in ϕ or k.

In summary, both SLIP and RTW are capable of achieving various gaits,

Table S1: Comparison between IP, SLIP, RW, RTW, and biomechanical models.

		Common gaits	Motion states						DOFs	Parameters	References
			NLSP	SLSP	DLSP	TLSP	QLSP	PLSP			
IP	Biped	Walking		○	—	—	—	—	1	3	[6]
	Quadruped			○	—	—	—	—		4	[21]
SLIP	Biped	Walking	○	○		—	—	—	2	6	[8, 9, 10]
		Running	○	○		—	—	—		5	
		Skipping	○	○		—	—	—		5	
		Jumping	○	○		—	—	—		5	
	Quadruped	Crawling		○	○	○	—	—	2	7	[11, 12, 13, 14]
		Walking		○	○	○	—	—		7	
		Trotting	○	○	○		—	—		6	
		Pacing	○	○	○		—	—		6	
		Galloping	○	○	○		—	—		6	
		Bounding	○		○		—	—		6	
	Hexapod	Tripod				○			2	7	[17, 18, 19]
		Tetrapod			○	○	○			8	
		Wave		○	○	○	○	○		9	
		Crawling		○	○	○	○	○		9	
RW		Walking		○	—	—	—	—	3	3	[7]
RTW		Skipping	○	○			—	—	9	6	
		Walking		○	○		—	—			
		Crawling			○	○	—	—			
Biomodel	Horse	Trotting	○	○	○		—	—	10	30	[1]
		Galloping	○	○	○		—	—			[2]
	Frog	Jumping	○	○		—	—	—	6	24	[3]

while IP, RW, and biomechanical models are designed to generate primarily a single gait. The SLIP models have been widely used by many researchers due to their inherent simplicity. To realize physically realistic gait (considering collisions) with, *e.g.*, asymmetric movements, additional parameters are required with their values carefully chosen. Simulation of switching between different gaits should be even more difficult. The RTW has a higher DOF, which increases the computational cost. It however has fewer parameters and only a slight change in one of the parameters can switch the gaits.

References

[1] H. M. Herr and T. A. McMahon, "A trotting horse model," *The International Journal of Robotics Research*, vol. 19, no. 6, pp. 566–581, 2000.

[2] ——, "A galloping horse model," *The International Journal of Robotics Research*, vol. 20, no. 1, pp. 26–37, 2001.

[3] M. Wang, X.-z. Zang, J.-z. Fan, and J. Zhao, "Biological jumping mechanism analysis and modeling for frog robot," *Journal of Bionic Engineering*, vol. 5, no. 3, pp. 181–188, 2008.

[4] C. M. Bishop and N. M. Nasrabadi, *Pattern recognition and machine learning*. Springer, 2006, vol. 4, no. 4.

[5] V. Vapnik, *The nature of statistical learning theory*. Springer science & business media, 2013.

[6] S. Kajita, M. Morisawa, K. Miura, S. Nakaoka, K. Harada, K. Kaneko, F. Kanehiro, and K. Yokoi, "Biped walking stabilization based on linear inverted pendulum tracking," *2010 IEEE/RSJ International Conference on Intelligent Robots and Systems*, pp. 4489–4496, 2010.

[7] T. McGeer, "Passive dynamic walking," *The International Journal of Robotics Research*, vol. 9, no. 2, pp. 62–82, 1990.

[8] U. Saranlı, Ö. Arslan, M. M. Ankaralı, and Ö. Morgül, "Approximate analytic solutions to non-symmetric stance trajectories of the passive spring-loaded inverted pendulum with damping," *Nonlinear Dynamics*, vol. 62, pp. 729–742, 2010.

[9] I. Uyanık, Ö. Morgül, and U. Saranli, "Experimental validation of a feed-forward predictor for the spring-loaded inverted pendulum template," *IEEE Transactions on robotics*, vol. 31, no. 1, pp. 208–216, 2015.

[10] H. Yu, H. Gao, and Z. Deng, "Toward a unified approximate analytical representation for spatially running spring-loaded inverted pendulum model," *IEEE Transactions on Robotics*, vol. 37, no. 2, pp. 691–698, 2020.

[11] G. Garofalo, C. Ott, and A. Albu-Schäffer, "Walking control of fully actuated robots based on the bipedal slip model," *2012 IEEE International Conference on Robotics and Automation*, pp. 1456–1463, 2012.

[12] M. Shahbazi, R. Babuška, and G. A. Lopes, "Unified modeling and control of walking and running on the spring-loaded inverted pendulum," *IEEE Transactions on Robotics*, vol. 32, no. 5, pp. 1178–1195, 2016.

[13] Z. G. Zhang, Y. Fukuoka, and H. Kimura, "Stable quadrupedal running based spring-loaded two-segment legged on a model," *IEEE International Conference on Robotics and Automation, 2004. Proceedings. ICRA'04. 2004*, vol. 3, pp. 2601–2606, 2004.

[14] M. H. Raibert, "Trotting, pacing and bounding by a quadruped robot," *Journal of biomechanics*, vol. 23, pp. 79–98, 1990.

[15] R. J. Full and D. E. Koditschek, "Templates and anchors: neuromechanical hypotheses of legged locomotion on land," *Journal of experimental biology*, vol. 202, no. 23, pp. 3325–3332, 1999.

[16] U. Saranli, M. Buehler, and D. E. Koditschek, "Design, modeling and preliminary control of a compliant hexapod robot," *Proceedings 2000 ICRA. Millennium Conference. IEEE International Conference on Robotics and Automation. Symposia Proceedings (Cat. No. 00CH37065)*, vol. 3, pp. 2589–2596, 2000.

[17] R. Altendorfer, U. Saranli, H. Komsuoglu, D. Koditschek, H. B. Brown, M. Buehler, N. Moore, D. McMordie, and R. Full, "Evidence for spring loaded inverted pendulum running in a hexapod robot," *Experimental Robotics VII*, pp. 291–302, 2001.

[18] T.-T. Lee, C.-M. Liao, and T.-K. Chen, "On the stability properties of hexapod tripod gait," *IEEE Journal on Robotics and Automation*, vol. 4, no. 4, pp. 427–434, 1988.

[19] M. Schilling, T. Hoinville, J. Schmitz, and H. Cruse, "Walknet, a bio-inspired controller for hexapod walking," *Biological cybernetics*, vol. 107, pp. 397–419, 2013.

[20] A. Goswami, B. Thuilot, and B. Espiau, "Compass-like biped robot part i: Stability and bifurcation of passive gaits," Ph.D. dissertation, INRIA, 1996.

[21] T. M. Griffin, R. P. Main, and C. T. Farley, "Biomechanics of quadrupedal walking: how do four-legged animals achieve inverted pendulum-like movements?" *Journal of Experimental Biology*, vol. 207, no. 20, pp. 3545–3558, 2004.